Available online at www.sciencedirect.com

ScienceDirect

Procedia Structural Integrity 42 (2022) 1008–1016

Structural Integrity Procedia

www.elsevier.com/locate/procedia

23 European Conference on Fracture - ECF23

Fatigue life assessment in the very high cycle regime of AISI 316L stainless steel processed by L-DED additive manufacturing

M. F. Andrade[a]*, M. V. Pereira[a], M. C. Teixeira[a], A. T. Junior[b], J. Gutjar[c]

[a]*Pontifícia Universidade Católica do Rio de Janeiro, Departamento de Engenharia Química e de Materiais, Rua Marques de São Vicente, 255, Rio de Janeiro, 22453-901, RJ, Brazil.*
[b]*Universidade Federal de Santa Catarina, PPG em Engenharia e Ciências Mecânicas, Rua Dona Francisca, 8300, Joinville, 89219-600, SC, Brazil.*
[c]*Universidade Federal de Santa Catarina, PPG em Engenharia Mecânica, Rua Lauro Linhares, 1850, Florianópolis, 88070-260, SC, Brazil.*

Abstract

Additive manufacturing technologies have arisen great industrial interest for manufacture of components and final parts intended for applications in several sectors of the industry. Most of these components are designed to have a service life greater than 10^7 cycles, making the analysis of the fatigue behaviour in the very high cycle regime (VHCF) an essential design criterion. The 316L stainless steel is one of the most processed and discussed in the literature. However, there is still no consolidated knowledge about the fatigue life of this material manufactured by different available techniques and their respective mechanisms of initiation of cracks predominant in the VHCF regime. The present work is intended for an experimental study of the VHCF failure mechanism of AISI 316L steel after additive manufacturing by laser directed energy deposition. In order to also identify the effect of post-processing steps, two different conditions of the material (as built and heat treated) were analysed. The specimens were submitted to ultrasonic tests with a target number of 10^9 cycles, at a frequency of 20±0,5 kHz and R=-1. The fracture surfaces were analysed later and the influence of heat treatment on the population of metallurgical defects, "fish-eye" formation and material's fatigue life were verified.

Keywords: L-DED; Ultrasonic fatigue; Crack initiation

*Corresponding author.
E-mail address: matheus-fernandes-andrade@outlook.com

10.1016/j.prostr.2022.12.127

1. Introduction

Due to the increasing technological development resulting from the last decades, there is a strong demand for equipment with greater efficiency, productivity and long service lives. Starting from the beginning, additive manufacturing technologies have aroused great interest in several sectors of the industry. Where often components are designed to have a fatigue life that exceeds 107 cycles. For this reason, for these applications the analysis of fatigue behavior in the very high cycle fatigue regime (VHCF) has become one of the main design criteria (EPMA (2015), Miedzinski (2017)).

There are different additive manufacturing technologies for metallic materials, but L-DED (Laser Directed Energy Deposition) technology has become very promising for a number of applications in the aerospace, automotive and medical industries. In addition to being a process that has great flexibility in terms of the feed material (metallic powder or filler wire), it also allows the manufacture of multifunctional 3D components from different materials simultaneously (EPMA (2015), Miedzinski (2017), Gibson et al. (2010) and Mahamood (2018)). According to Sabbori et al. (2020) a range of materials can be used in this process, but AISI 316L stainless steel is one of the most investigated and processed by these techniques due to the excellent mechanical properties that are preserved in the final parts.

Many researchers have evaluated the influence of process parameters on the characteristics, properties and microstructure of the final parts. Yadollahi et al. (2015) investigated the influence of the time interval between the deposition of layers on the mechanical properties and microstructural evolution. The relationship between mechanical properties and microstructural evolution with process parameters was also addressed by Sun et al. (2019), however, considering the effect of laser power, metallic powder feed rate, scanning speed and chemical composition of different metallic powders. It can be also cited the research by Ribeiro et al. (2020), Zheng et al. (2019), Tan et al. (2019), Majumdar et al. (2005) and Zietala et al. (2016). Ribeiro et al. verified the influence of different deposition strategies and spacing between the deposition beads on the surface roughness, density and hardness of the material, Zheng et al. investigated the variation of laser power and working distance on surface quality, mechanical properties, microstructure and internal defects, Tan et al. studied the correlation between porosity, density and final microstructure, Majumdar et al. and Zietala et al. evaluated the effect of process parameters (laser power, scan speed, powder feed rate and deposition direction) on mechanical properties, microstructure and corrosion resistance.

Despite all the advantages, L-DED is also reported by Sabbori et al. (2020), Mahamood (2018), Gibson et al. (2010) and Miedzinski (2017) and other researchers as an extremely sensitive technique to process parameters. Laser power, hatch spacing, scan speed, powder feed rate, deposition pattern, building atmosphere, and other parameters exert a strong influence on the final properties parts, where an undesired parameters combination can generate internal defects in the manufactured material. Typical defects produced by this technology are pores, voids, metallic inclusions, lack of fusion, among others. Several authors reported that all these mentioned defects favor the crack nucleation process in VHCF regimen (Sabbori et al. (2020), Bathias (2005), Pyttel at al. (2011), Bathias et al. (2001), Kazymyrovych (2010) and Marines et al. (2003)).

Nomenclature

σa	Applied stress amplitude
σu	Ultimate strength
σy	Yield strength
N_f	Number of cycles to failure
AB	As built
HT	Heat treated
FGA	Fine granular area

In VHCF regimen, different from what is seen in conventional regimes, the crack tends to start preferably in the internal region or in subsurface regions from defects present in the material. This fact leads to the formation of a characteristic morphology on the fracture surface, known as “fish-eye”. The “fish-eye” corresponds to a circular area, generally with a diameter varying between (0.5 to 1 mm), concentric to the origin of the fault, formed from the radial propagation of the crack. The formation of this morphology is considered an evaluation parameter of the fatigue failure process in the VHCF regime. The crack evolution process in this case occurs in four stages: nucleation/initial crack growth, growth inside the fish-eye, growth outside the fish-eye and final fracture (Bathias (2005), Kazymyrovych (2009)).

Another phenomenon also observed at the fracture surface, more specifically within the fish-eye region, is the formation of a fine granular area (FGA) around the crack initiation sites. The FGA has a characteristic roughness that is distinct from the rest of the fracture surface (Bathias (2005), Pyttel et al. (2011), Kazymyrovych (2009)).

Although AISI 316L stainless steel is one of the most related in the literature, there is still no consolidated knowledge about fatigue life and the predominant mechanisms of crack initiation in the VHCF regime of this material after AM. For this reason, this work was aimed at an experimental study of the failure mechanism in VHCF of AISI 316L steel processed by L-DED. In order to also verify the effect of the post-processing steps, two conditions of the material, as built (AB) and heat treated (HT), were evaluated.

2. Material and Experimental Procedure

2.1 Material

The metallic powder used for the confection of all specimens was a gas atomized 316L stainless steel powder (code 316L-5520), made by Höganäs company. Table 1 shows the chemical composition of 316L-5520 powder, as well as the maximum and minimum concentration for each chemical element as specified by ASTM A276 (2013).

Table 1. Chemical composition (wt%) of 316L stainless steel (316L-5520).

	C	Si	Mn	Cr	Mo	Ni	Fe
316L-5520	0,019	0,7	1,5	16,9	2,5	12,7	68,47
ASTM A276 (*max*)	0,030	1,00	2,00	16,0 -18,0	2,0 - 3,0	10,0 -14,0	Bal

The powder particles are shown in Figure 1. Based on scanning electron microscopy (SEM) analysis it is observed that the particles are predominantly spherical, with granulometric distribution of 53-150 μm. It is also seen the presence of asymmetrical morphologies as well as agglomerates of particles called "satellites". According to Sabbori et al. (2020) and Markusson (2017) the formation of this kind of particle is due to the atomization process, where during solidification small particles tend to adhere to the surface of larger ones.

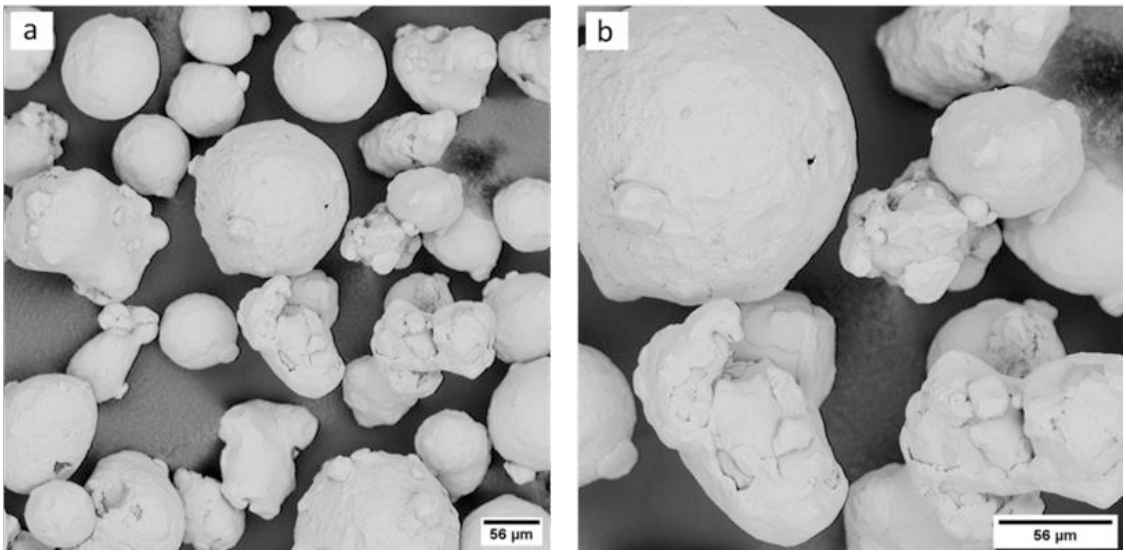

Fig. 1. SEM image of 316L - 5520 powder. a) Magnification 500x; b) Magnification 2000x. (Adapted from Thiesen (2021)).

2.2 Description of the Manufacturing Process

The AISI 316L stainless steel specimens were manufactured in cylindrical bars shape (117 mm in length and 18 mm in diameter). For that, it used an RPM Innovations 535 machine with a 25° nozzle. All specimens were vertically built using the same process parameters, which are indicated in Table 2.

Table 2. L-DED process parameters (Thiesen, (2021)).

Laser power (W)	Spot size (mm)	Scanning speed (mm/min)	Feed Rate (g/min)	Carrier gas flow (L/min)	Shielding gas flow (L/min)	Hatch spacing (mm)	Oxygen level (ppm)
1300	1,78	1446	30	6	40	1,223	< 50

In order to evaluate the influence of post-processing steps in the manufacturing process, heat treatments (stress relief followed by a solubilization) were carried out on some samples. The stress relief treatment were carried out at 550°C for 6 hours and cooled in air. In the solubilization, these samples were kept at 1070°C for 2 hours (1 hour for a soak), and cooled in saline solution until 260°C and then in air until the room temperature. Therefore, two conditions of the material (as-built and heat treated) were analyzed in this research.

Tensile tests were carried out in three samples of each material's condition. The tests were performed on Instron 5988 equipment, according to the ASTM A370. The tensile test results for both material's condition in comparison to what is specified by ASTM A276 (2013) are shown in Table 3.

Table 3. Tensile test results for both material's condition.

Condition	σu (MPa)	σy (MPa)	Elongation (%)
As-built	604,7 / 1,25	380,7 / 1,89	45,7 / 6,85
As-built + HT	575, 3 / 1,25	298 / 0,82	53,7 / 0,47
ASTM A276	485	170	40

The material's density was measured by Archimedes's method and a value of 7,91 g/cm³ was obtained for this physical property. As the heat treatments carried out are not specific for density increase, this property remained unchanged for both conditions.

2.3 VHCF tests

All VHCF tests were conducted in the LABFADAC's laboratory of the PUC-Rio University in Brazil using a Shimadzu USF-2000 ultrasonic machine (frequency = 20 kHz), shown in Figure 2. The specimens of both conditions were tested at R= -1. The ultrasonic machine is composed of four main components: a power generator that transform 50 to 60 Hz voltage signal into 20 kHz ultrasonic electrical sinusoidal signal, a piezoelectric converter that is responsible to transform the electrical signal into longitudinal ultrasonic waves and vibration (mechanical loading) of the same frequency, an ultrasonic horn that amplifies the vibration coming from the piezoelectric converter in order to obtain the required strain amplitude, in the middle section of the specimen and a computer monitoring and data acquisition system.

Fig. 2. Shimadzu USF-2000 ultrasonic machine at LABFADAC's laboratory.

The specimen used in VHCF tests is designed to present the natural frequency at 20 kHz (the same frequency used in the test) and for that, it must be dimensioned by its resonance length (L_1). This specimens' dimension is influenced by physical properties of the material such as dynamic modulus of elasticity (Ed) and density (ρ) and could be explained by the longitudinal elastic waves theory and calculated by equations developed by Bathias (2005). Figure 3 presents the geometry used for both conditions and the dimensions in which the specimens were machined.

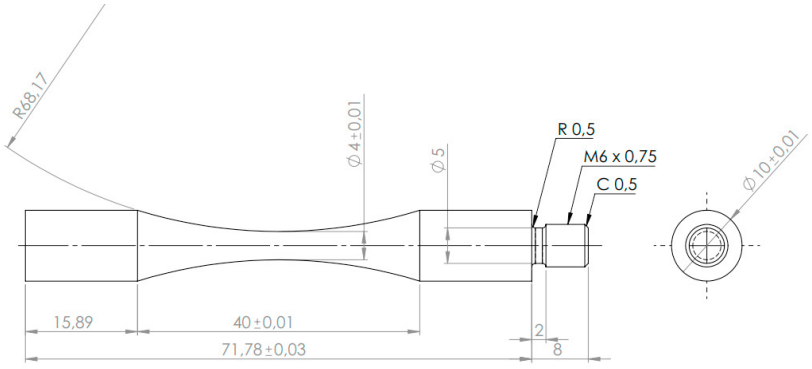

Fig. 3. Hourglass shape specimens with dimension in mm.

After the tests the samples were statically disrupted and their fracture surfaces were investigated by scanning electron microscopy (SEM).

3. Experimental Results

3.1 S-N curve

Figure 4 presents the plotted S-N data for both conditions of specimens. As shown, all the experiments were carried out aiming 1.0E+09 cycles (run out).

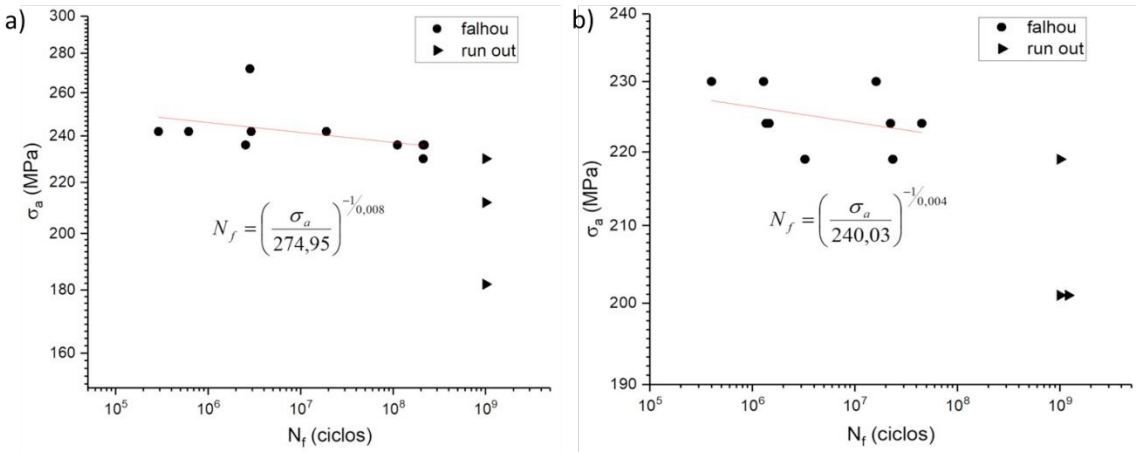

Fig. 4. S-N data of: a) AB 316L (AM) specimens and b) HT 316L (AM) specimens.

There was a great dispersion in the results related to the number of cycles to failure of the specimens tested in the same stress amplitude, however such dispersion was already expected.

In general, analysing all the cases in which the comparison between the conditions was made by relativizing the LRM percentages to values corresponding to stress amplitudes, it was observed that the AB condition presented better results. For example, for stresses corresponding to 39% of the ultimate strength, the specimens of the HT condition presented a fatigue life around (1.0E+06 – 1.0E+07) cycles, while for the AB condition, the fatigue life predominantly exceeded 1.0E+08 cycles.

3.2 Fractographic analysis

All fracture surfaces of the specimens that failed the fatigue tests were analysed by SEM, and it was verified that for both conditions, non-metallic inclusion were the mandatory defects that acted as crack initiation sites. Three specimens were selected to be presented. Table 4 summarizes the information of each specimen labeled 1 to 3 with the applied stress amplitude (σ_a) and corresponding fatigue life (*Nf*). It is noteworthy that the formation of fish-eye and FGA was verified only for the heat treated specimens.

Table 4. Specimens selected for fractographic analysis.

Specimens nº	Condition	σ_a (MPa)	N_f (cycles)
1	AB	236	1.11E+08
2	HT	219	2.34E+07
3	HT	224	2.22E+07

The crack initiation sites were observed in Figures 5-7 and details of fish-eye and FGA formation are observed in Figures 6 and 7.

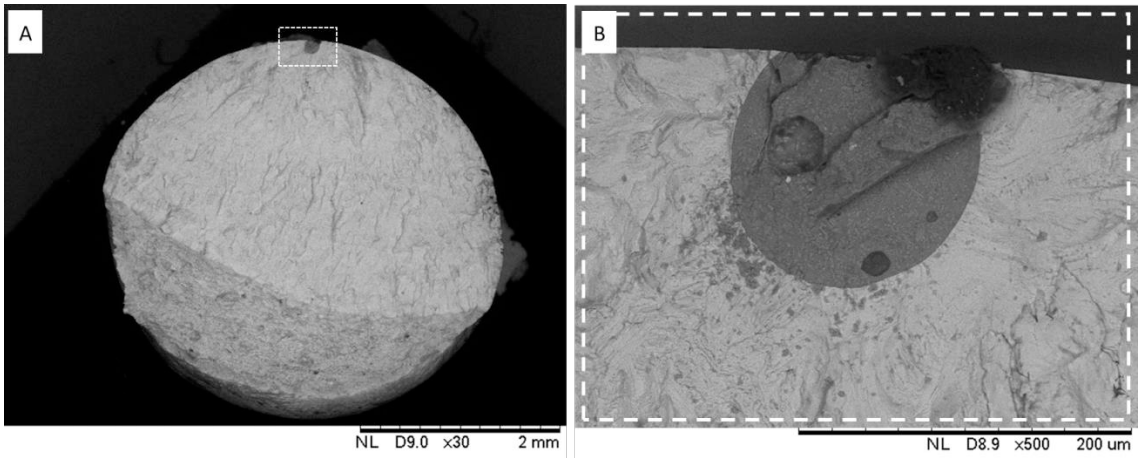

Fig. 5. SEM of fracture surface of specimen n° 1: a) Fracture surface; b) Magnification of crack nucleation site.

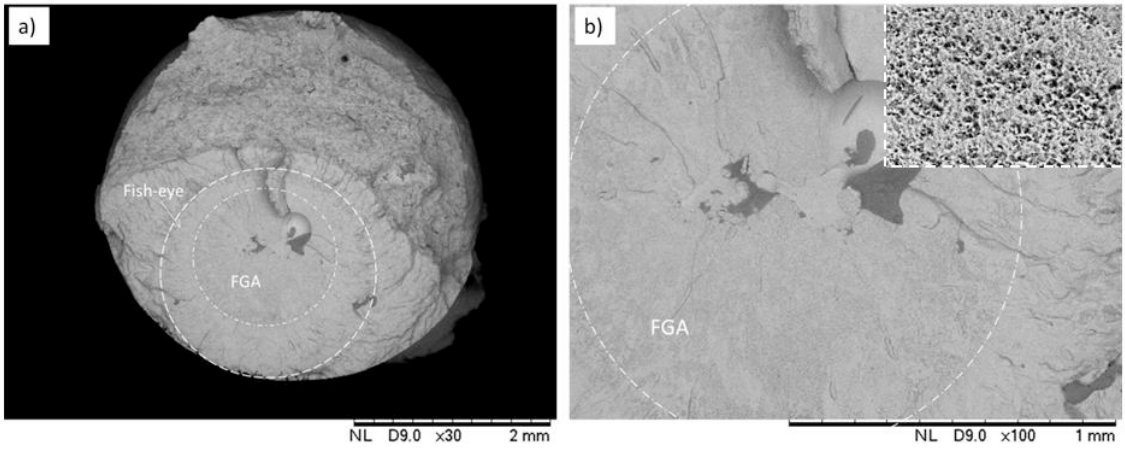

Fig. 6. SEM of fracture surface of specimen n° 2: a) Fish-eye formation; b) Magnification of FGA area with fine grain detailed (Andrade et al. (2022)).

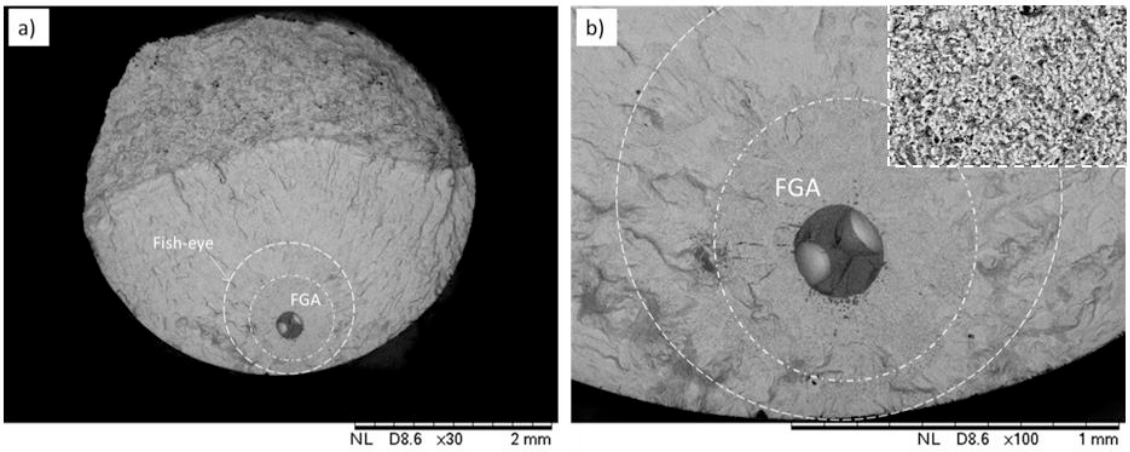

Fig. 7. SEM of fracture surface of specimen nº 3: a) Fish-eye and FGA formations; b) Magnification of FGA area with fine grain detailed (Andrade et al. (2022)).

4. Conclusions

The present work evaluated two post-processing conditions, with and without heat treatment, of AISI 316L steel manufactured by L-DED. The results obtained allowed the following conclusions:

- Regarding the ultrasonic tests, it was observed that the AB condition presented better performance. Considering that the stress amplitude of the tests was relativized with percentages of the mechanical strength limit, all AB specimens presented higher fatigue resistance.
- The heat treatments used (stress relief and solubilization) were not effective in prolonging the fatigue life of the material.
- From the experimental data, the recommended working stresses for the AB and HT condition are equivalent to 212 MPa and 201 MPa, respectively.
- The fatigue strength for 1E+09 corresponds to 35% of the LRM for both material conditions. This fact is consistent with what is found in the literature regarding the resistance to conventional fatigue for this given number of cycles.
- The formation of internal and subsurface fish-eye was observed only in the specimens of the HT condition. Although their dimensions are different, it was possible to verify the limits and characteristics of the FGA formed around the initiation sites and to prove that the roughness in both situations is similar.

Acknowledgments

This work was developed in partnership with SENAI Institute of Innovation in Manufacturing Systems and Laser Processing, FIESC-SENAI/SC. The authors would like to thank FAPERJ (Fundação de amparo a pesquisa do estado do Rio de Janeiro) for the financial support through project n.2021/00674-8.

References

ASTM (American Society for Testing and Materials). 2013. “Standard Specification for Stainless Steel Bars and Shapes, ASTM A276”. p. 2.

Andrade, M. F., Teixeira, M. C., Pereira, M. V. 2022. “Experimental study of VHCF fractographic features of conventionally and additively manufactured steels”. *Journal of Materials Research and Technology* (submitted July 28, 2022 – status: Awaiting Reviewer Scores).

Bathias, C., Drouillac, L., Le François, P. 2001. “How and why the fatigue SN curve does not approach a horizontal asymptote”. *International Journal of Fatigue*, vol. 23, pp. S143-S151.

Bathias, C., Paris, P. C. 2005. “Gigacycle fatigue of mechanical practice”. New York: Marcel Dekker Inc.

EPMA. 2015. “Introduction to additive manufacturing technology: a guide for designers and engineer”. Shrewsbury, UK, 1st ed.

Gibson, I., Rosen, D. R., Stucker, B. 2010. “Additive Manufacturing Technologies – Rapid prototyping to Direct Digital Manufacturing”. New York: Springer.

Kazymyrovych, V. 2009. “Very High Cycle Fatigue of engineering materials – A literature review”. Karlstad University Studies.

Kazymyrovych, V. 2010. “Very High Cycle Fatigue of tool steel”. Karlstad University Studies.

Mahamood, R. M. 2018. “Laser Metal Deposition Process of Metals, Alloys and Composite materials”. Manchester, UK: Springer.

Majumdar, J. D., Pinkerton, A.; Liu, Z.; Manna, I.; Li, L. 2005. “Mechanical and electrochemical properties of multiple-layer diode laser cladding of 316L stainless steel”. *Applied Surface Science*, 247(1-4):373–377.

Marines, I., Bin, X., Bathias, C. 2003. “An understanding of very high cycle fatigue of metals*”. International Journal of Fatigue*, vol. 25, pp. 1101-1107.

Markusson, L. 2017. “Powder Characterization for Additive Manufacturing Processes,” Luleå. University of Technology.

Miedzinski, M. 2017. “Materials for Additive Manufacturing by Direct Energy Deposition – Identification of materials properties that can have an influence on the building process or the resulting component properties”. Chalmers University of Technology.

Pyttel, B., Schwerdt, D., Berger, E. C. 2011. “Very High Cycle Fatigue - Is there a fatigue limit?”. *International Journal of Fatigue*, vol. 33, pp. 49-58.

Ribeiro, K. S. B., Mariani, F. E., Coelho, R. T. 2020. “A study of different deposition strategies in direct energy deposition”. *Procedia Manufacturing*, 48:663-670.

Sabbori, A., Aversa, A., Marchese, G., Biamino, S., Lombardi, M., Fino, P. 2020. “Microstructure and mechanical proprieties of AISI 316L Produced by Direct Energy Deposition-Based Additive Manufacturing: A Review”. *Applied sciences*, 10, 3310.

Sun, G. F., Shen, X., Wamg, Z., Zhan, M., Yao, S., Zhou, R., Ni, Z. 2019. “Laser metal deposition as repair technology for 316L stainless steel: Influence of feeding powder compositions on microstructure and mechanical properties”. *Optics and Laser Technologies*, 109:71-83.

Tan, Z.E., Pang, J. H. L., Kaminski, J., Pepin, H., Zhi’en, E. T. 2019. “Characterisation of porosity, density, and microstructure of directed energy deposited stainless steel AISI 316L”. Additive Manufacturing, 25:286-296.

Thiesen Jr, A. 2021. “Selection of processing parameters for the laser directed energy deposition process applied to additive manufacturing: a methodological proposal”. [Dissertation]. Joinville: UFSC.

Yadollahi, A., Shamsaei, N., Thompson, S. M., Seely, D. W. 2015. “Effects of process time interval and heat treatment on the mechanical and microstructural properties of direct laser deposited 316L stainless steel”. *Materials Science and Engineering A*, 644:171–183.

Zheng, B., Haley, J. C., Yang, N., Yee, J., Terrassa, K. W., Zhou, Y., Lavernia, E. J., Schoenung, J. M. 2019. “On the evolution of microstructure and defect control in 316L SS components fabricated via directed energy deposition”. *Materials Science and Engineering A*, 764:138243.

Zietala, M. et al. 2016. “The microstructure, mechanical properties, and corrosion resistance of 316L stainless steel fabricated using laser engineered net shaping”. *Materials Science and Engineering A*, 677: 1-10.